# A combined transformation of ordering SPECT sinograms for signal extraction from measurements of Poisson noise

Hongbing Lu*, Dongqing Chen, Lihong Li, Guoping Han, and Zhengrong Liang
Department of Radiology, State University of New York, Stony Brook, NY 11794, USA

## ABSTRACT

A theoretically based transformation, which reorders SPECT sinograms degraded by the Poisson noise according to their signal-to-noise ratio (SNR), has been proposed. The transformation is equivalent to the maximum noise fraction (MNF) approach developed for Gaussian noise treatment. It is a two-stage transformation. The first stage is the Anscombe transformation, which converts Poisson distributed variable into Gaussian distributed one with constant variance. The second one is the Karhunen-Loeve (K-L) transformation along the direction of the slices, which simplifies the complex task of three-dimensional (3D) filtering into 2D spatial process slice-by-slice. In the K-L domain, the noise property of constant variance remains for all components, while the SNR of each component decreases proportional to its eigenvalue, providing a measure for the significance of each components. The availability of the noise covariance matrix in this method eliminates the difficulty of separating noise from signal. Thus we can construct an accurate 2D Wiener filter for each sinogram component in the K-L domain, and design a weighting window to make the filter adaptive to the SNR of each component, leading to an improved restoration of SPECT sinograms. Experimental results demonstrate that the proposed method provides a better noise reduction without sacrifice of resolution.

Keywords: SPECT sinogram, Poisson noise reduction, K-L transformation, Anscombe transformation, Wiener filter, adaptive filtering

## 1. INTRODUCTION

As a "direct" estimation of source activity distribution from observed projection data in SPECT (singe photon emission computed tomography), fully iterative reconstruction algorithms have been developed, such as maximum-likelihood expectation maximization (ML-EM) [1], maximum *a posteriori* probability EM (MAP-EM) [2], penalized weighted least squares (WLS) [3], and the like. They represent an optimal solution to their objective criteria, respectively, with the options of compensating for photon attenuation and scattering, collimator/detector blurring, and statistical variability simultaneously. The results of these approaches are promising, but the computational burden is high and many questions regarding regularization and convergence remain unsolved. The straightforward filtered backprojection (FBP) reconstruction is currently widely used, but it lacks quantitative capability, carrying artifacts due to the attenuation and resolution variation. An FBP-type analytical inversion reconstruction with compensation for the photon attenuation and resolution variation can be as accurate as the fully iterative algorithms at the similar computing efficiency as the straightforward FBP, if the Poisson noise is effectively treated [4]. That means, if we can estimate the true projection data from the observed ones, image reconstruction then can be proceeded by means of an FBP-type algorithm, which can achieve quantitative accuracy as fully iterative methods and computational efficiency as analytical inversions [5,6].

Poisson noise is one of the major factors that degrade the quality of SPECT and must be treated first before any analytical reconstruction algorithm is applied. It is well known that Poisson noise varies depending on the intensity at each voxel (signal dependence) [7], rendering a very challenging task to noise reduction for analytical approach to the quantitative SPECT. Various forms of filtering techniques have been developed to spatially filter images corrupted by this type of noise [7-12]. Some of these techniques lie in the specification of a non-stationary model for the description of the noise, resulting in non-stationary filters that operate independently at each pixel [7-9]. Nevertheless, the formulation of the model is difficult, if not impossible, in the low-count SPECT situation. In order to satisfy the WLS criterion with Gaussian noise model, Fessler *et al* [3] proposed a curve-fitting strategy on each projection to minimize a roughness-penalized, WLS objective function, in which the weights were inversely proportional to the data values. But the WLS component of the objective function is optimal only for normally distributed data with unequal known variances, and the iterative image reconstruction process is time consuming. Recently, La Riviere *et al* [10] developed a smoothing approach in the sinogram space in which a non-parametric regression

* Correspondence: hblu@clio.rad.sunysb.edu; phone 1 631 444-2736; fax 1 631 444-6450; http://www.sunysb.edu/micl/; State University of New York, Stony Brook, NY, USA 11794

using a roughness-penalized Poisson likelihood objective function is used to smooth each projection independently. The approach was found to have desirable uniform and isotropic resolution and yield resolution-noise tradeoffs superior to those shift-invariant filtering techniques on the projection images. Although the simulation results are promising, the iterative smoothing needs more computing effort and the adjustable smoothing parameter is undetermined. Another approach of Pelegrini *et al* [11,12], which is very similar to our work, applies square-root transformation to projection data first and then smoothes the transformed curve by the use of a statistical technique known as the fixed-effect model. The similarities and differences between this approach and ours will be discussed in greater detail in Section 4.

To some degrees, the restoration of SPECT sinograms from measurements is mathematically similar to that of restoring multi-spectral and color images, a quite active research topic in the past two decades [13-17]. Hunt and Kubler [13] first applied the K-L (Karhunen-Loeve, also called principal components) transformation to decompose the multi-spectral Wiener filtering process into single spectral filtering. The inability of the K-L transformation to reliably separate signal and noise components of remote-sensing multi-band image data has led to the development of the MNF (maximum noise fraction) transform [14]. It was derived as an analogue of the K-L transform, where the criterion for the generation of the components is to maximize the noise content represented by each component, rather than the data variance. In reverse order these components maximize the SNR (signal-to-noise ratio) represented by each component [14]. Lee *et al* [15] further described the MNF transform as a transformation of the data to a coordinate system in which the noise covariance matrix is the identity matrix, followed by a principal components transformation. They refereed it as a noise-adjusted principal components (NAPC) transform [15]. Application of these transforms requires knowledge of the signal and noise covariance matrices of the data, which generally is not directly available. Although the method for estimating signal covariance is apparent, the method for estimating noise covariance is not, especially in noisy SPECT projection images. Wernick *et al* [18-20] has applied K-L domain Wiener filter to dynamic PET (positron emission tomography) by the assumption that the blur in the sinogram is space-invariant and the noise is approximately white. They further discarded the higher order K-L components to improve the computational speed. This approach is very effective for noise reduction and, therefore, should be practically useful for the smoothing of projection images if the two assumptions of white noise and discarded components containing no information are valid. In clinic situations with SPECT modality, these assumptions are often invalid.

In this paper, we propose a theoretically based transformation, which reorders the SPECT sinograms according to their SNR, for an adaptive filtering of the projection data degraded by the Poisson noise. We show below that our method is equivalent to a two-stage transformation: first the data are transformed by Anscombe transform so that the noise covariance matrix is a constant identity matrix, then the K-L transform is applied along the direction of the slices. By applying this combined transform, we can construct an accurate 2D Wiener filter for each sinogram component in the K-L domain, and design a weighting window to make the filter adaptive to SNR of each component, leading to an improved restoration of SPECT projection images.

## 2. METHODS

### 2.1. Anscombe transformation

The task of spatial filtering of signal-dependent Poisson noise can be greatly simplified by applying the Anscombe transformation to all the sinogram data, which converts Poisson distributed noise into Gaussian distributed one with constant variance. That is, if $x$ is Poisson distributed with mean equal to $\lambda$, then $y= (x+3/8)^{1/2}$ can be approximated as Gaussian distributed with its mean equal to $(\lambda+1/8)^{1/2}$ and its variance equal to 0.25 [21-23]. Therefore, by Anscombe transformation, the noise becomes signal independent and the noise model can be expressed as:

$$\boldsymbol{g' = f' + n'} \tag{1}$$

where $\boldsymbol{g'} = [y_1^T\, y_2^T \ldots y_K^T]^T$, $\boldsymbol{f'} = [f'_1{}^T\, f'_2{}^T \ldots f'_K{}^T]^T$, $\boldsymbol{n} = [n_1^T\, n_2^T \ldots n_K^T]^T$. and $g'_i$, $f'_i$, and $n'_i$ $(i=1,2,\ldots,K)$ denote a $M\times 1$ vector obtained by lexicographically ordering the transformed sinogram data, the "true" sinogram (to be estimated), and the noise, respectively, for slice $i$. Notice that here $n'_{i;j}$ is Guassian noise with constant variance $0.25$. In this situation, the noise covariance matrix is the identity matrix (unit variance and no correlation) multiplied by $0.25$.

### 2.2. K-L transformation along the direction of the slices

Applying K-L transform along the direction of the slices, the K-L basic vectors then can be obtained as the eigenvectors of the covariance matrix $K_t$ $(K\times K)$ between different slices or sinograms [13,16], i.e., they are the row of matrix $A$ defined by

$$K_t A^T = A^T D \tag{2}$$

where $D = diag\{d_1,\ldots,d_K\}$ and $d_i$ is the $i$-th eigenvalue of $K_t$.

The K-L transformation of the whole projection data along the direction of the slices then can be represented by a matrix $A_M$ of the following form [16]

$$A_M = A \otimes I_M = \begin{bmatrix} \begin{bmatrix} a_{11} & & 0 \\ & \ddots & \\ 0 & & a_{11} \end{bmatrix} & \begin{bmatrix} a_{12} & & 0 \\ & \ddots & \\ 0 & & a_{12} \end{bmatrix} & \cdots & \begin{bmatrix} a_{1K} & & 0 \\ & \ddots & \\ 0 & & a_{1K} \end{bmatrix} \\ \begin{bmatrix} a_{21} & & 0 \\ & \ddots & \\ 0 & & a_{21} \end{bmatrix} & \ddots & & \vdots \\ \vdots & & \ddots & \vdots \\ \begin{bmatrix} a_{K1} & & 0 \\ & \ddots & \\ 0 & & a_{K1} \end{bmatrix} & \cdots & \cdots & \begin{bmatrix} a_{KK} & & 0 \\ & \ddots & \\ 0 & & a_{KK} \end{bmatrix} \end{bmatrix} \tag{3}$$

in which $A_{ij}$ represents the elements of the matrix $A$, $I_M$ denotes the $M \times M$ identity matrix and $\otimes$ represents the Kronecker product. From the structure of $A_M$, it can be seen that all pixels in the same slice are subject to the same transformation.

Apply $A_M$ to Anscombe transformed projection data $\boldsymbol{y'}$, then the K-L transformation and its inverse one can be defined as

$$\text{K-L transform:} \quad \boldsymbol{y} = A_M \boldsymbol{g'} \tag{4}$$

$$\text{Inverse K-L transform:} \quad \hat{\boldsymbol{g}} = A_M{}^T \boldsymbol{y}. \tag{5}$$

The covariance matrix of projection data along the direction of the slices can be estimated from [13]

$$K_{t;kl} = \frac{1}{M-1} \sum_{i=1}^{M} (g'_{k,i} - \bar{g}_k)(g'_{l,i} - \bar{g}_l) \tag{6}$$

where

$$\bar{g}_k = \frac{1}{M} \sum_{i=1}^{M} g'_{k,i}, \quad k,l = 1,\ldots,K \tag{7}$$

Rewrite Eq.(4), we have

$$\boldsymbol{y} = A_M \boldsymbol{g'} = A_M \boldsymbol{f'} + A_M \boldsymbol{n'} = \boldsymbol{y}_1 + \boldsymbol{n}_1 \tag{8}$$

where $\boldsymbol{y}_1 = A_M \boldsymbol{f'}$, and $\boldsymbol{n}_1 = A_M \boldsymbol{n'}$.

### 2.3. Wiener filtering in K-L domain

In this section, we will formulate a Wiener filter in K-L domain after Anscombe transformation. Corresponding to Eq.(1), the MMSE or Wiener restoration is produced by [16]

$$\hat{\boldsymbol{f}}' = K_{f'}(K_{f'} + K_{n'})^{-1} \boldsymbol{g'} \tag{9}$$

where $K_{f'}$ and $K_{n'}$ are the covariance matrices of the signal and noise after Anscombe transformation, respectively.

To simplify the 3D restoration problem, we assume that $K_{f'}$, the spatial covariance matrix, can be separated into two components as follows:

$$K_{f'} = K_t \otimes K_s. \tag{10}$$

where $K_t$ is the covariance matrix among slices and $K_s$ is the covariance matrix of those within a slice. The validation of the separatibility assumption has been discussed in [13]. Usually, it can be applied directly to imaging of motion-free objects. It is noted that this assumption is one basis for the following models of this paper.

Applying Wiener filter restoration upon the transformed data in Eq.(8), the restoration can be written as

$$\hat{\boldsymbol{y}}_1 = K_{y1}(K_{y1} + K_{n1})^{-1} \boldsymbol{y} \tag{11}$$

where $K_{n1}$ is the covariance matrix of the transformed noise and $K_{y1}$ is one of the transformed projection data $\boldsymbol{y}_1$. To calculate

$\boldsymbol{y}_1$, we have

$$K_{y1} = E[\boldsymbol{y}_1 \boldsymbol{y}_1{}^T] = E[A_M \boldsymbol{f'f'}^T A_M{}^T] = A_M K_{f'} A_M{}^T$$
$$= (A \otimes I_M)(K_t \otimes K_s)(A \otimes I_M)^T = AK_t A^T \otimes Ks \,. \tag{12}$$

Considering the definition of the K-L matrix $A$ in Eq.(2), we have $AK_t A^T = D$, and this yields

$$K_{y1} = D \otimes K_s \tag{13}$$

which is block diagonal in the K-L domain.

Similarly, we can obtain the covariance matrix of noise $n_1$

$$K_{n1} = E[\boldsymbol{n}_1 \boldsymbol{n}_1{}^T] = E[A_M \boldsymbol{n'n'}^T A_M{}^T] = A_M K_n A_M{}^T . \tag{14}$$

After Anscrombe transform, the Poisson distributed data become approximately Guassian distributed with the variance equal to 0.25, thus $K_{n'}$ can be simply expressed as $\sigma_n^2 (I_M \otimes I_K)$, where $\sigma_n^2$ is a constant equal to 0.25. By substituting $K_{n'}$ in Eq.(14), we have

$$K_{n1} = (A \otimes I_M)(\sigma_n^2 I_M \otimes I_K)(A \otimes I_M)^T = \sigma_n^2 (A A^T \otimes I_M) = \sigma_n^2 I_K \otimes I_M , \tag{15}$$

which demonstrates that the noise property of constant variance remains for all components in the K-L domain.

Examining Eq.(11), we see that all the indicated matrices are block diagonal. Thus, the Wiener filter of Eqn.(11) can be expressed as K independent filters of each component, as shown below

$$\hat{\boldsymbol{y}}_{1i} = d_i K_s (d_i K_s + \sigma_n^2 \boldsymbol{I}_M)^{-1} \boldsymbol{y}_i \qquad , i=1, 2, \ldots, K \tag{16}$$

If we assume spatial stationarity for each sinogram component, the 2D Wiener filter in the K-L domain would be

$$H(\omega_s, k_\theta) = \frac{S_{y_i}(\omega_s, k_\theta) - \sigma_n^2}{S_{y_i}(\omega_s, k_\theta)} \tag{17}$$

where $S_{yi}$ is 2D discrete Fourier transform (FT) of K-L domain data $\boldsymbol{y_i}$ at the point $(s,\theta)$ of slice $i$, and $\sigma_n^2$ is the constant noise variance equal to *0.25*. The availability of the noise covariance matrix in this method eliminates the difficulty of separating noise from signal.

### 2.4. The relationship between the eigenvalues and the SNR of sinograms

Since the noise and signal components of the projections are uncorrelated, the covariance matrix of the signal $K_{f'}$ is given by:

$$K_{f'} = K_{g'} - K_{n'} \tag{18}$$

Then the task becomes to find a transform with vectors, $a_i$, which maximizes the SNR [14]:

$$SNR = \frac{a_i^T K_{f'} a_i}{a_i^T K_{n'} a_i} = \frac{a_i^T K_{g'} a_i}{a_i^T K_{n'} a_i} - 1 \tag{19}$$

On the other hand, after Anscombe transform, $K_{n'} = 0.25\, I$. Rewrite Eq.(19), we have:

$$SNR + 1 = 4 \frac{a_i^T K_{g'} a_i}{a_i^T a_i} . \tag{20}$$

It is well know that the K-L basic vectors (the eigenvectors) of the covariance matrix $K_{g'}$ maximize the above equations. After we apply K-L transform on all projection data slice by slice, we have $a_i{}^T K_{g'} a_i = d_i \otimes K_s$, where $d_i$ is the $i$th eigenvalue of $K_t$, and $a_i{}^T a_i = 1$. Then it can be seen that $SNR + 1 = 4\, d_i \otimes K_s$, which means that the SNR of K-L domain sinogram components can be reflected by the eigenvalues of the transformed sinogram covariance matrix. This provides one measure of the significance of the components in K-L domain. In another words, performing K-L transformation slice-by-slice makes each K-L domain component independent and the SNR of each component decrease monotonically for lower eigenvalues.

Above we showed the relationship between the eigenvalues and component SNR. It should be noted that this SNR is over the entire sinograms, and a component that is very significant in a small area of the sinogram could have an eigenvalue close to one (SNR $\approx$ 0) [14]. In general, although the higher order K-L components contain more noise, they still contain noticeable signal constituent, and discarding them could generate artifacts (as observed by many researchers). If these signals

need to be retained, each K-L component must be filtered before inverse transformation to obtain a cleaned image.

To further improve the performance of the filtering, a weighting window could be applied to make the filter adaptive to sinogram SNR. The weighting given to the areas with lower SNR should be lessened, while areas with higher SNR should be enhanced, in order to preserve edge information and reduce the noise. There are many methods to design the weighting window [24], while most of them are selected to be functions of the eigenvalues. In section 3 we show a realization of the weighting window and its performance on noise reduction by using the Metz window [25].

As the lower order components concentrate the major information while the higher order components have a significant noise fraction, we can select a special value of the eigenvalues, for example, 1, as the threshold. For components with eigenvalues greater than the threshold, slightly filtering or no filtering procedures should be applied to reserve the information. In the mean time, intense filtering procedures can be applied to other components, without serious degradation to the signal content of the image, to improve the filtering performance.

## 3. EXPERIMENTAL RESULTS

### 3.1. Experimental preparation

Two experimental 3D anthropomorphic head phantoms were used to simulate radiotracer distributions inside object-specific attenuating media for evaluation of different filtering techniques. One is the RSD (Radiology Support Device, Inc., CA) Striatal head phantom that includes four small compartments (two for nucleus caudate of 5.4 ml and two for putamen of 6.0 ml) in a brain volume of 1,250 ml surrounded by skull and scalp enclosure. The other is the Hoffman brain model that has detailed structures for white matter, gray matter, and CSF (cerebrospinal fluid) embedded in a plastic cylinder with 1,050 ml air space inside (Data Spectrum, Inc., NC).

A triple-head parallel-hole collimated SPECT system was employed to acquire emission data using a triple energy-window acquisition protocol for attenuation/scatter correction. The Striatal phantom with 4:1 activity ratio between the four small compartments and the brain volume was scanned for six times, three clockwise and three counter-clockwise. All the projection data were sampled on a grid of 128×128, with 128 views evenly spanned on a circular orbit of 360°. For Hoffman phantom scan, 1,050 ml water mixed with 15mCi Tc-99m was injected into the air space. The phantom is designed to achieve a 4:1 ratio between gray matter/CSF and white matter. It was scanned for three times. The projection data were sampled on a grid of 128×128 per view over 120 views evenly spanning on 360°. Emission images were reconstructed by the conventional FBP method after different kinds of noise filtering. To get noise-free image for comparison purpose, we added all projection data obtained from different heads and different scans together and treated the reconstructed image as the approximated noise-free one. The 53rd slice image of the Striatal phantom reconstructed from the averaged projection data is shown at the left-top of Figure 1, while the approximated noise-free slice images 57, 67, 70, and 74 of the Hoffman phantom is shown at the top row in Figure 2.

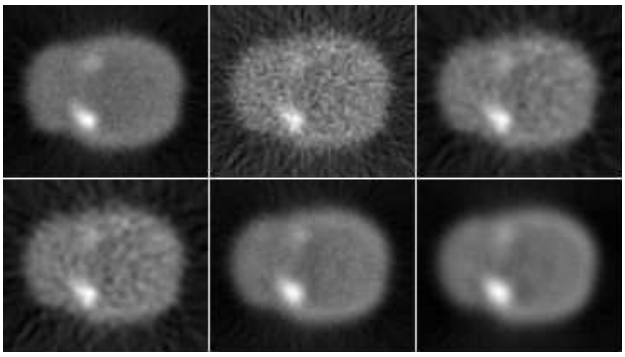

**Figure 1**. Reconstructed slices of the Striatal phantom data filtered by different filtering approaches. From left to right: on the top are approximated noise-free and noisy data with Ramp and Hanning; on the bottom are Shepp-Logan, proposed method, and 3D Wiener filter (without K-L transformation and adaptive weighting).

### 3.2. Experimental results

The reconstructed transverse slices of the Striatal phantom projection data filtered by different filtering approaches are shown in Figure 1, while the reconstructed slices of the Hoffman phantom data are shown in Figure 2. The cutoff frequencies for

Hanning and Shepp-Logan filters are 0.5 and 0.35, respectively. The reconstructed images filtered by the Hanning or the Shepp-logan filter reveal insufficient noise suppression. In the mean time, those filtered by direct Anscombe transform + 3D Wiener filter (without K-L transformation and adaptive weighting) show a little over-smoothed. This is because of the stationary assumption, which is required by the 3D Wiener filtering and is not correct for the whole projection data set, especially around the edge and boundary of the object. The proposed K-L domain noise-adjusted Wiener filtering demonstrates a better noise reduction without sacrifice of resolution.

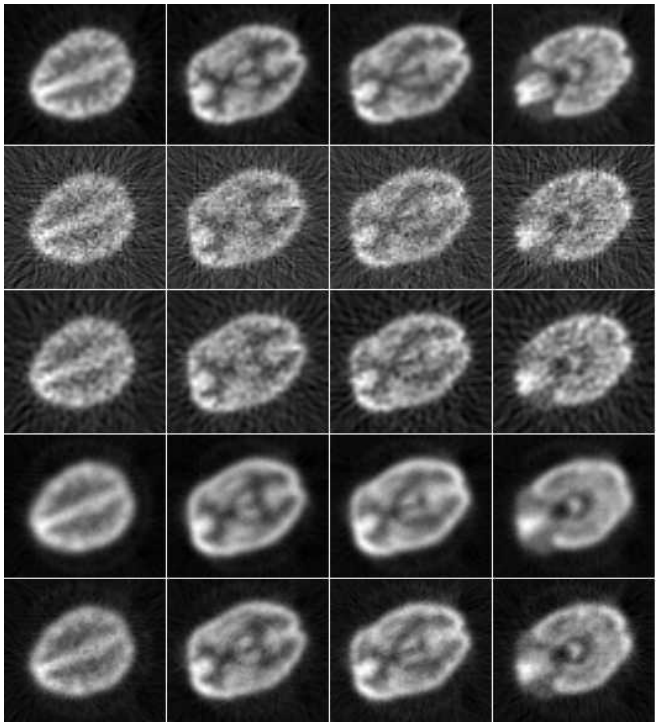

**Figure 2**. Reconstructed slices of the Hoffman phantom data filtered by different filtering approaches. From left to right: slice 57, 67, 70, 74. From top to bottom: approximated noise-free, noisy data by Ramp, Hanning, 3D Wiener filter (without K-L transformation and adaptive weighting), and proposed method.

Application of the proposed transform to the Hoffman phantom experimental data yielded the component images as shown in Figure 3. The superior performance of this combined transformation on all ordered components in terms of image quality is apparent. It can be seen that in the 22nd component, there still has noticeable spatial information, visible out of the noise.

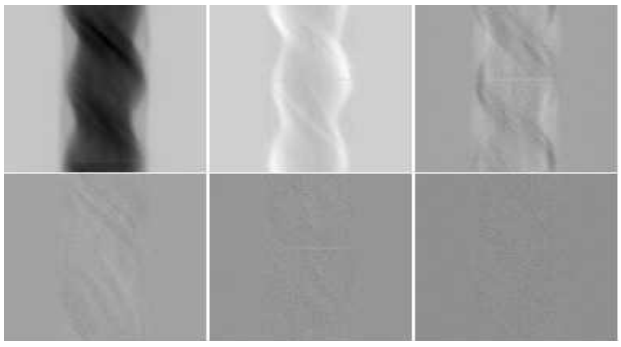

**Figure 3**. K-L domain component images (sinograms). From left to right: on the top are K-L sinogram 1, 2, and 5; on the bottom are K-L sinogram 10, 22, and 65.

Figure 4 shows the effect of different filtering method in the K-L domain. On the second row, we selected a threshold of 1.0. For those components with eigenvalues greater than 1.0, we simply keep them without filtering. For other components, the K-L domain Wiener filter (without the weighting window) was applied. The third row of that figure demonstrates the K-L

Wiener filtering with adaptive weighting window. We selected the Metz window as weighting scale [25], adaptive to the eigenvalue of each component (SNR). The weighting window was applied on each K-L domain sinogram during Wiener filtering. Reconstructed images filtered with the K-L domain Wiener filter using weighting window show a better filtering effect as compared with that using a simple threshold.

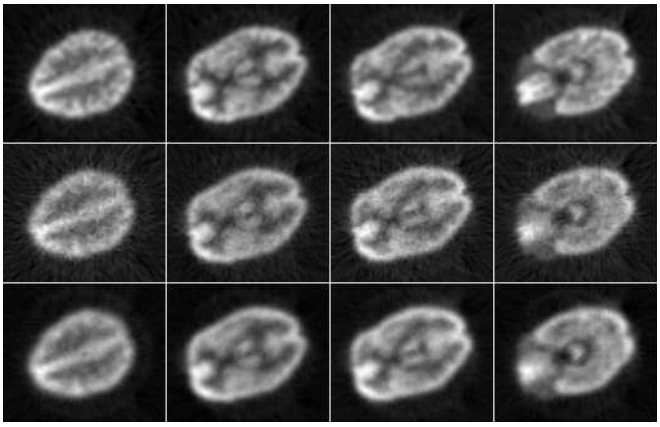

**Figure 4**. Reconstructed slices of the Hoffman phantom data filtered by different filtering approaches. From left to right: slice 57, 67, 70, and 74. From top to bottom: approximated noise-free, selected filtering, and K-L domain adaptive filtering.

## 4. DISSCUSSION AND CNONCLUSION

The proposed method provides an optimal treatment of the projection data with Poisson noise. It is composed of two transformations: one is the Anscombe transform for noise identification, and the other is the K-L transform for ordering the sinograms in terms of image quality, followed by adaptive filtering in the K-L domain. This combined transformation is equivalent, in some degrees, to the MNF transform for multi-spectral data and is optimal in the sense that it maximizes the SNR in each successive transform components, similar to the K-L transform which maximizes the data variance in successive components. The availability of the noise covariance matrix eliminates the theoretical difficulty of separating noise from signal for sinal-dependent noisy data. The effectiveness of the proposed method for signal-to-noise improvement is demonstrated with two brain phantom experimental studies. The experimental results demonstrate that the proposed filtering method has a better performance on noise removal than conventional filters do, and can preserve more edge information as compared to 3D global Wiener filtering, due to the K-L adaptive filtering.

In the non-parametric regression sinogram smoothing proposed recently by La Rivière *et al* [10], a roughness-penalized Poisson likelihood objective function was used. By trying three different link functions, which generally are used to express the roughness penalty, they found that the choice of the link function has a significant influence on the resolution uniformity and isotropy properties of the reconstructed images. Especially, the choice of a square-root link function yielded the desirable outcome of essentially uniform and isotropic resolution in the reconstructed images, better than other two link functions of the identity and logarithm links. That choice also rendered a superior performance for noise smoothing as compared to that of the Hanning filtering as well as that of the WLS approach. The use of the square-root link function seems to be similar to our use of the Anscombe transform, but there is an important difference. The Anscombe transform can approximate, in a high accuracy, the Poisson distributed variables into normally distributed ones, while the square-root link function can not. Theoretically the fitting of the link function in the exact Poisson likelihood in the objective function is attractive, but the iterative process and existence of free-adjustable parameters need more attention for practical applications. In our recent work, we also investigated the resolution uniformity and isotropy properties of the K-L and Anscombe transforms. The preliminary results were very encouraging, demonstrating desirable uniform and isotropic resolution in the reconstructed images. In fact, for the space-invariant tomographic data as considered in this study, the resolution non-uniformity arises from the non-uniform variance of the Poisson noise. Fessler *et al* [3,26] has shown qualitatively that non-uniform weighting is essential to achieve the desirable noise properties of statistic methods.

The regularized backprojection method (RBP) proposed by Pelegrini et al [11,12] takes the advantage of the space correspondence theorem and involves two stages. First, a statistical model is used to estimate the noise-free part of the projections. In this stage, Anscombe transform is first applied on acquired projection data, then the estimated noise-free part is obtained by solving a minimization problem by a spline smoothing (the smooth parameter $\gamma$ controls the smoothness of the

functions). A principal component analysis of smoothing spline functions is applied along the direction of the bins and the subspace is spanned by the first Q eigenvectors associated with the largest Q eigenvalues. Thus the filtered projections belong to a subspace of the Sobolev space which the acquired projections belong to. In the second stage, the filtered projections are reconstructed using spline filtered backprojection which ensures that the reconstructed object belongs to a space consistent with that containing the projections. Though both of us utilize the Anscombe transform and K-L transform, the objective is completely different. They use the two transforms to obtain filtered projections that belong to a subspace of the Sobolev space which the acquired projections belong to, while we use them to obtain ordering sinograms according to their SNR in the K-L domain for a better noise reduction. Secondly, the main problem in their method is how to determine a combination of [$\gamma$, Q] that would provide a better noise/resolution trade-off than optimized FBP reconstruction, for any object and noise level, which is definitely not necessary in our method. Furthermore, the K-L transform may be performed along the ordering of detector bins, or rotation angles, or image slices. We have applied it along different directions [27]. Our recent simulation results on the local impulse response of reconstructed images demonstrated the influence of the direction of K-L transform and the number of principal components on the resolution uniformity. To keep the resolution uniformity in 95% confidence interval, more than 85 K-L components (from a total of 128) would be required for the K-L transform along the ordering of bins, while only 35 components would be required for the ordering of slices. This result may provide another criterion for the determination of parameter Q. The alternative implementation of FBP called spline-filtered backprojection (SFBP) proposed by them also could potentially be incorporated into our approach. The appeal of SFBP is that it ensures that the regularity properties of the projections are carried into the reconstructed image, avoiding the small shift-variance introduced by the conventional discretization in FBP reconstruction [10-12].

Considering the restoration of gated cardiac SPECT that attracts more research efforts recently, it suggests rather positive prospect to apply the proposed method to the spatio-temporal filtering problem, which is currently under investigation in our group [28].

## ACKNOWLEDGEMENTS

This work was partially supported by NIH Grant #HL54166 of the National Heart, Lung and Blood Institute; Grant #NS33853 of the National Institute of Neurological Disorder and Stroke; and the Established Investigator Award of the American Heart Association.

## REFERENCES

1. L.A. Shepp and Y. Vardi, “Maximum likelihood reconstruction for emission tomography,” *IEEE Transactions on Medical Imaging*, **1**, pp.113-122, 1982.
2. E. Levitan and G.T. Herman, “A maximum a *posteriori* probability expectation maximization algorithm for image reconstruction in emission tomography”, *IEEE Transactions on Medical Imaging*, **6**, pp.185-192, 1988.
3. J.A. Fessler, “Penalized weighted least-squars image reconstruction for positron emission tomography,” ,” *IEEE Transactions on Medical Imaging*, **13**, pp.290-300, 1994.
4. S.J. Glick, B.C. Penney, M.A. King, and C.L. Byrne, “Non-Iterative Compensation for the Distance-Dependent Detector Response and Photon Attenuation in SPECT Imaging”, *Conf Record IEEE Med Imaging*, **2**, pp.1172-1174, 1993.
5. Z. Liang, J. Ye, J. Cheng, and D.P. Harrington, "Quantitative Brain SPECT in Three Dimensions: an analytical approach to non-uniform attenuation without transmission scans," in *Computational Imaging and Vision book series*, by Kluwer Academic Publishers, pp.117-132, 1996.
6. J. You, Z. Liang, and G. Zeng, "A Unified Reconstruction Framework for Both Parallel-Beam and Variable Focal-Length Fan-Beam Collimators by a Cormack-Type Inversion of Exponential Radon Transform," *IEEE Transactions on Medical Imaging*, **18**, pp.59-65, 1999.
7. C.L. Chan, A.K. Katsaggelos, and A.V. Sahakian, “Image sequence filtering in quantum-limited noise with applications to low-dose fluoroscopy,” *IEEE Transactions on Medical Imaging*, **12**, pp.610-621, 1992.
8. C.L. Chan, A.K. Katsaggelos, and A.V. Sahakian “Linear-quadratic noise-smoothing filters for quantum-limited images”, *IEEE Transactions on Image Processing*, **4**, pp.1328-33, 1995.
9. D.T. Kuan, A.A. Sawchuk, T.C. Strand, and et al, “Adaptive noise smoothing filter for images with signal-dependent noise,” *IEEE Trans. Patt. Anal. Mach. Intel.*, **7**, pp.653-665, 1985.
10. P.J. La Rivière, and Xiaochuan Pan, “Nonparametric regression sinogram smoothing using a roughnes-penalized Poisson likelihood objective function”, *IEEE Transactions on Medical Imaging*, **19**, pp.773-786, 2000.
11. M. Pélégrini, H. Benali, G. El Fakhri, and et al, “ Two-dimensional statistical model for regularized backprojection in

SPECT", *Phys. Med. Biol*., **43**, pp.421-434, 1998.
12. M. Pélégrini, I. Buvat, H. Benali, and et al, " A spline-regularized minimal residual algorithm for iterative attenuation correction in SPECT", *Phys. Med. Biol*., **44**, pp.2623-2642, 1999.
13. B.R. Hunt, and O. Kübler, "Karhunen-Loeve Multi-spectral image restoration, part I: theory," *IEEE Transactions on Acoustics, Speech, and Signal Processing*, **ASSP-32**, pp.592-600, 1984.
14. A.A. Green, M. Berman, P. Switzer, and M.D. Craig, " A transformation for ordering multispectral data in terms of image quality with implications for noise removal," *IEEE Transactions on Geosci. Remote Sensing, 26*, pp.65-74, 1988.
15. J.B. Lee, A.S. Woodyatt, and M. Berman, "Enhancement of high spectral resolution remote-sensing data by a noise-adjusted principal components transform," *IEEE Transactions on Geosci. Remote Sensing*, **28**, pp.295-304, 1990.
16. M.K. Özkan, A.T. Erdem, M.I. Sezan, and et al. "Efficient multiframe Wiener restoration of blurred and noisy Image sequences. *IEEE Transactions on Image Processing*, **1**, pp.453-475, 1992.
17. A.K. Katsaggelos, K.T. Lay, and N.P. Galatsanos, "A General framework for frequency domain multi-channel signal processing," *IEEE Transactions on Image Processing*, **2**, pp.417-420, 1993.
18. M.N. Wernick, E.J. Infusino, and C.M. Kao, "Fast optimal pre-reconstruction filters for dynamic PET," *1997 IEEE Conference Record of the NSS and MIC*, 1997.
19. M.N. Wernick, E.J. Infusino, and M. Milosevic, "Fast Spatio-temporal image reconstruction for dynamic PET," *IEEE Transaction on Medical Imaging*, **18**, pp.185-195, 1999.
20. M.V. Narayanan, M.A. King, E.J. Soares, and et al, "Application of the Karhunen-Loeve Transform to 4D Reconstruction of cardiac gated SPECT images," *IEEE Transaction on Nuclear Science*, **46**, pp.1001-1008, 1999.
21. F.J. Anscombe, "The transformation of Poisson, binomial and negative-binomial data,"*Biometrics*, **35**, pp.246-254, 1948.
22. J.H. Cheng, Z. Liang, J. Ye, and et al, "Inclusion of a Priori information in frequency space for quantitative SPECT imaging," *1996 IEEE Conference Record of the NSS and MIC*, 1996.
23. J.H. Cheng, *Frequency-domain approaches to quantitative brain SPECT*, Ph.D. Thesis, Dept. of Radiology and Computer Science, State University of New York at Stony Brook, 1997.
24. F.J. Harris, "On the use of windows for harmonic analysis with the discrete Fourier transform," *Proceedings of the IEEE*, **66**, pp.51-83, 1978.
25. M.A. King, P.W. Doherty, R.B. Schwinger, and et al, "Fast count-dependent digital filtering of nuclear medicine images: Concise communication", *J. Nuclear Medicine*, **24**, pp.1039, 1988.
26. J.A. Fessler, and W.L. Rogers, "Spatial resolution properties of penalized-likelihood image reconstruction: space-invariant tomographs", *IEEE Transactions on Image processing*, **5**, pp.1346-1358, 1996.
27. H. Lu, G. Han, D. Chen, L. Li, and Z. Liang, "A Theoretically Based Approach to Noise Reduction in SPECT by Anscombe and K-L Transforms", *J. Nuclear Medicine*, **41**, pp.198P, 2000.
28. H. Lu, G. Han, D. Chen, and et al, "A theoretically based pre-reconstruction filter for spatio-temporal noise reduction in gated cardiac SPECT", *2000 IEEE Conference Record of the NSS and MIC*, 2000.